NANO LETTERS

pubs.acs.org/NanoLett

Letter

Stimulated Emission through an Electron–Hole Plasma in Colloidal CdSe Quantum Rings

Carmelita Rodà, Bastiaan B. V. Salzmann, Isabella Wagner, Yera Ussembayev, Kai Chen, Justin M. Hodgkiss, Kristiaan Neyts, Iwan Moreels, Daniel Vanmaekelbergh, and Pieter Geiregat*

Cite This: *Nano Lett.* 2021, 21, 10062–10069

Read Online

ACCESS | Metrics & More | Article Recommendations | Supporting Information

ABSTRACT: Colloidal CdSe quantum rings (QRs) are a recently developed class of nanomaterials with a unique topology. In nanocrystals with more common shapes, such as dots and platelets, the photophysics is consistently dominated by strongly bound electron–hole pairs, so-called excitons, regardless of the charge carrier density. Here, we show that charge carriers in QRs condense into a hot uncorrelated plasma state at high density. Through strong band gap renormalization, this plasma state is able to produce broadband and sizable optical gain. The gain is limited by a second-order, yet radiative, recombination process, and the buildup is counteracted by a charge-cooling bottleneck. Our results show that weakly confined QRs offer a unique system to study uncorrelated electron–hole dynamics in nanoscale materials.

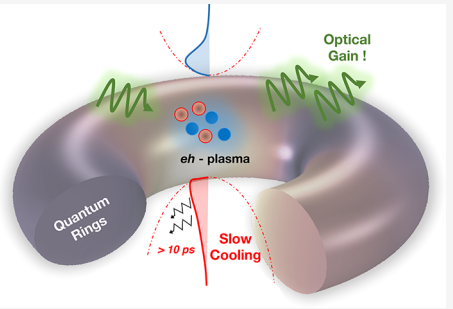

KEYWORDS: *nanostructures, 2D materials, spectroscopy, stimulated emission, quantum rings*

In the past decade, Cd-based nanocrystals with variable degrees of confinement have been developed through colloidal synthesis procedures.[1,2] The ability to tune the nanocrystal shape has led to materials with remarkable optical properties. Nanoplatelets, for example, show anisotropic emission,[3] giant modal gain coefficients,[4,5] and record low gain thresholds[6] due to the presence of excitons, electron–hole pairs bound by strong Coulomb attractions, that are stable even at high densities.[7] However, all of these shapes are topologically equivalent with a genus of zero. An interesting new topology with a genus of one for Cd-based nanocrystals was put forward by Fedin et al., who synthesized toroidally shaped CdSe nanocrystals, also called quantum rings (QRs).[8] Starting from CdSe nanoplatelets, a thermochemical reconfiguration in the presence of selenium (Se) resulted in the formation of thin toroids.[8,9] The few optical studies on QRs have thus far been performed in the regime of a single electron–hole pair per ring, where likely excitons are the dominant charge species. Even in this regime, the QRs already display interesting properties such as broken rotational symmetry.[10] A single study on ultrafast time scales indicated strong coupling of single electron–hole pairs to surface defects and fast charge trapping.[11] To date, however, nothing is known on the nature of elementary excitations in QRs at increasing pair density. As a consequence, various interesting high-density effects remain unexplored, such as exciton-unbound charge carrier balances,[5,7,12] multicarrier recombination mechanisms,[13] carrier cooling[7,14,15] and potential stimulated emission.[4,16,17]

In this work, we combine femtosecond transient absorption and photoluminescence spectroscopy to study the photophysics of high-quality CdSe QRs over a full range of densities (i.e., from single up to 35 excitations per QR). First, we show that the used QR synthesis leads to limited ultrafast carrier trapping and pristine fast hole cooling at low carrier density, providing an intrinsic test bed for exploring QR properties. Next, we show that the dominant species at increasing carrier densities are unbound electron–hole pairs condensed into a plasma state which give rise to a sizable optical gain window. The latter is strongly red-shifted from the absorption spectrum due to band gap renormalization and remains broadband due to the absence of residual exciton absorption lines. In the QRs studied here, recombination at increasing carrier density is dominated by a cooling bottleneck at early times, followed by a fast yet radiative second-order recombination.

Figure 1a shows an electron microscopy image (HAADF-STEM) of the QRs which were synthesized using a modified procedure from Fedin et al.,[8] where the QRs are obtained starting from 4.5 monolayer (ML) CdSe nanoplatelets (Supporting Information).[9] As shown in the schematic of Figure 1a, the geometry of our QRs is best described as a single torus with outer dimensions L_x = 12.7 ± 6.0 nm and L_y = 10.3 ± 3.1 nm and an average in-plane width of w = 3.7 ± 0.9 nm. The thickness in the direction orthogonal to the ring plane

Received: September 30, 2021
Revised: November 17, 2021
Published: November 29, 2021

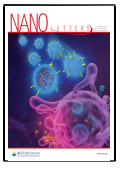

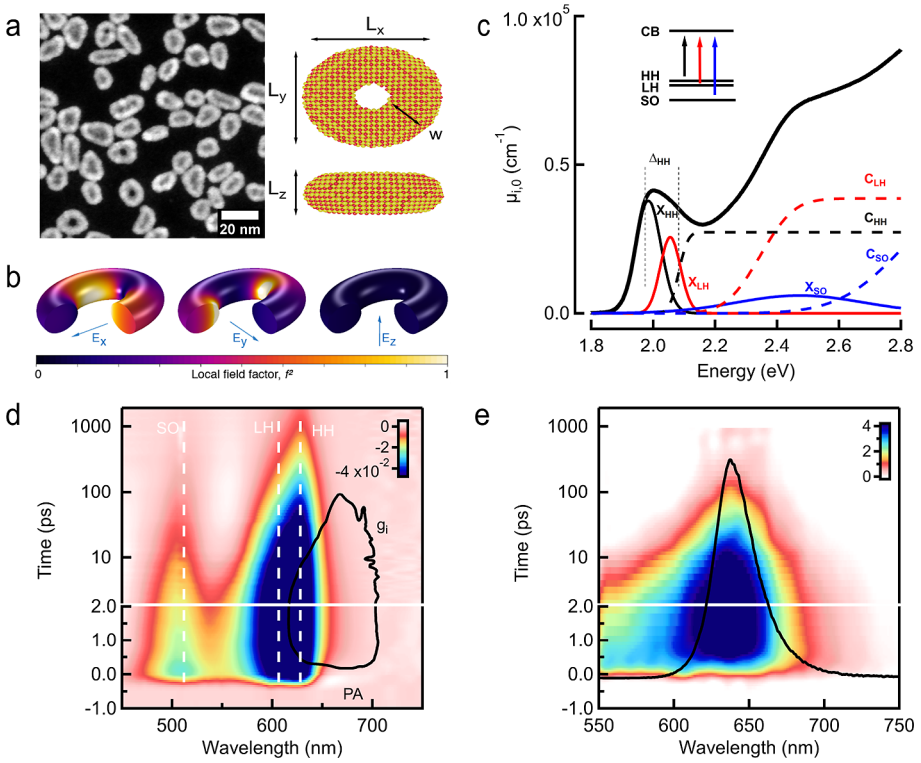

Figure 1. Overview of CdSe quantum rings. (a) HAADF-STEM imaging of the quantum rings (QRs) used in this work and a schematic depiction of a single QR with average outer in-plane dimensions of L_x = 12.7 nm and L_y = 10.3 nm and a thickness of L_z = 2.8 nm. (b) Numerical calculation of the distribution of the squared local field factor f^2 in a CdSe QR for the external electric field (blue arrows) aligned along the in-plane x (left) and y (middle) directions and the out-of-plane z (right) direction. (c) Deconvolution of the (intrinsic) linear absorption spectrum $\mu_{i,0}$ using heavy-hole (HH, black), light-hole (LH, red), and spin−orbit split-off (SO, blue) exciton bands (solid), combined with free carrier contributions (dashed lines). A scheme of the ensuing optical transitions is shown in the inset. The binding energy Δ_{HH} of the HH exciton is extracted from this fit as 107 ± 1 meV. (d) Transient absorption map ΔA after photoexcitation at 510 nm (2.4 eV), creating an average number of electron−hole pairs $\langle N \rangle$ = 13.8. The distinct optical transitions identified in Figure 1c are indicated by the vertical white dashed lines. The black contour line indicates the time−wavelength range where the bleach $\Delta A = A - A_0$ exceeds the linear absorption A_0, thereby giving rise to a net optical gain ($A < 0$, $g_i > 0$, main text). (e) False color map of the PL under similar excitation conditions ($\langle N \rangle$ = 18.5) as (d). The black trace indicates the steady-state photoluminescence spectrum which is centered at 627 nm.

amounts to L_z = 2.8 ± 0.6 nm, which equates to nearly 8.5 ML of CdSe.[1,18]

Considering their complex shape, we first performed a numerical calculation to analyze the dielectric response of the QRs to an external electric field. For this, we use our method based on the quasi-static field approximation[19,20] (Supporting Information). In Figure 1b, we report the distribution of the local field factor, the ratio between the external and internal fields, inside the ring for the in-plane (x, y) and perpendicular (z) directions. Taking the integral of the local field distribution over the ring volume, we finally obtain that the linear intrinsic absorption coefficient $\mu_{i,0}$ at 309 nm amounts to 3.01 × 10^5 cm^{-1}, which allows us to normalize (gain) spectra further on and calculate the number of absorbed photons per QR $\langle N \rangle$ accurately.[21]

In Figure 1c, we report the full absorption spectrum which resembles that of 2D semiconductors with a staircase profile toward higher energy.[1,18] The band gap absorbance consists of a broad peak at ∼1.9 eV,[17] associated with heavy hole (HH) and light hole (LH) transitions, and a second feature at higher energy which we assign to transitions from the split-off valence band (SO) to the conduction band. Next, we proceed with a quantitative decomposition in Figure 1c using a series of step functions, describing free carrier absorption from a 2D continuum of states (C, dashed lines) and the associated exciton absorption peaks (X, solid lines).[9] Notably, the exciton position energies, HH−LH splitting and the SO−CB transition extracted from the fit, line up with the values reported for weakly confined NPLs thicker than 8.5 ML (2.3 nm) (Supporting Information).[18,22] Finally, we extract the exciton binding energy Δ_{HH} as 107 ± 1 meV, matching the trend for decreasing exciton binding energy for increasing thickness.[23] On the basis of both the model and geometrical description of the QRs, we can state that charges are only weakly confined in every direction for the QRs under study.

To study the charge carrier dynamics, we employ two ultrafast optical methods: transient absorption (TA) and femtosecond photoluminescence (fPL) spectroscopy. In both methods, a 110 fs pulse excites a colloidal dispersion of QRs. Next, a broadband scheme measures either the change in absorption $\Delta A = A - A_0$ due to the pump (TA) or the intensity of the luminescence (fPL).[24] We performed TA experiments pumping at 400, 510, and 625 nm adjusting $\langle N \rangle$ experimentally up to nearly 35. The fPL experiments were carried out by pumping at 515 nm, in a similar range of $\langle N \rangle$.

Figure 1d shows the result of a typical TA experiment (i.e., a time−wavelength map of the differential absorbance $\Delta A(\lambda, t)$) for excitation at 510 nm using a photon flux that creates $\langle N \rangle$ = 13.8 electron−hole pairs per QR. Two distinct bleach bands ($\Delta A < 0$) are observed around the SO/CB transition at 509

https://doi.org/10.1021/acs.nanolett.1c03501
Nano Lett. 2021, 21, 10062−10069

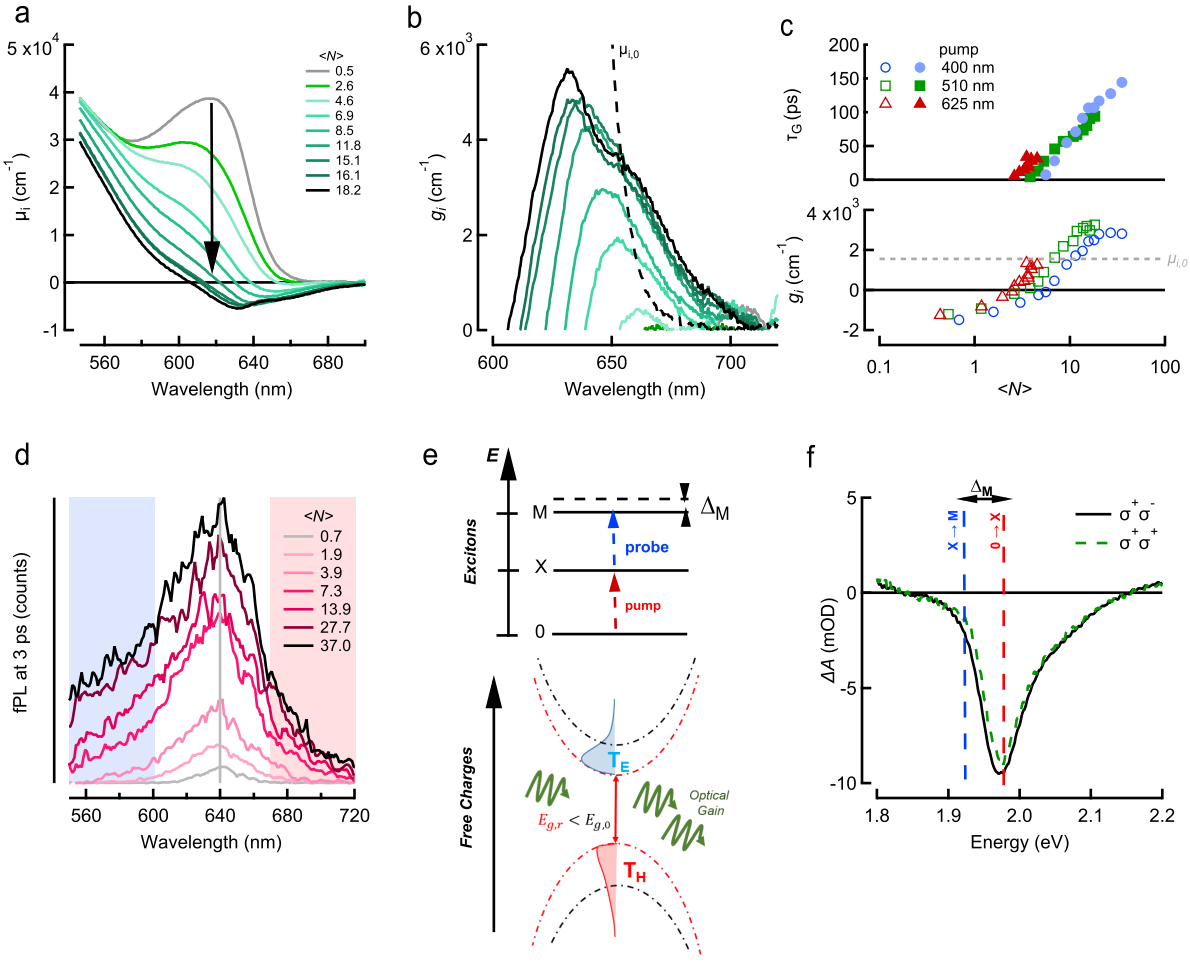

Figure 2. Gain spectroscopy of quantum rings. (a) Slices of the nonlinear intrinsic absorption μ_i at 3 ps after photoexcitation with 510 nm. The carrier density is expressed as $\langle N \rangle$. Note the collapse of the band edge absorption feature at 625 nm (vertical arrow) and the occurrence of net optical gain $\mu_i < 0$ beyond 600 nm. (b) Material gain g_i extracted from (a). The dashed line represents $\mu_{i,0}$ for the reference. (c) Material gain g_i (bottom) and gain lifetime τ_G (top) at 660 nm for increasing pair density and varying excitation wavelength: 400, 510, and 625 nm. The horizontal dashed gray line represents the value of $\mu_{i,0}$ at 660 nm. (d) Photoluminescence spectra for similar excitation conditions as in (a). Clear nonlinear increases on the low-energy (red shaded) and high-energy sides (blue shaded) are observed. (e) Gain models and an explanation of the photoinduced absorption in the exciton (top) and free charge carrier model (bottom). Dashed red bands indicate the red-shifted renormalized band gap $E_{g,r}$ relative to the linear gap $E_{g,0}$ (black dashed bands). (f) Polarization-resolved pump−probe spectroscopy using circularly polarized pump (σ^+) and probe (σ^+(green dashed)/σ^-(black)) sequences. Dashed vertical lines indicate the position of the ground-state exciton transition bleach (0 → X, red) and expected induced exciton-molecule transition (X → M, blue).

nm and around the band gap region at 620 nm. Pumping at 510 nm initially creates a hot hole in the SO valence band level and an electron in the lowest CB level (inset of Figure 1c). Focusing further on the band gap region at 620 nm, we observe a broadening at early times toward shorter wavelengths, which is absent at low pump power. At longer wavelengths (650−700 nm), a strong photoinduced absorption (PA, $\Delta A > 0$, white area) gives way to a broad bleach region below the band gap after ca. 1 ps. When comparing this to the linear absorption A_0, there is a region where ΔA exceeds A_0, giving rise to a net negative absorbance $A = \Delta A + A_0 < 0$ or optical gain. The time-wavelength region where this occurs is strongly red-shifted from the band gap transition and is indicated by the solid black contour line in Figure 1d. Figure 1e shows the result of the fPL experiment, where the luminescence is collected over a similar time−wavelength scale and for a similar carrier density ($\langle N \rangle = 18.5$) as for TA. It reveals time scales similar to those of TA and a broadening toward longer and shorter wavelengths compared to the steady-state PL (black, Figure 1e).

To analyze the optical gain development in more detail, we will use the absorbance $A(\lambda, t) = \Delta A + A_0$, which we normalize to represent the intrinsic absorption $\mu_i(\lambda, t)$. First, we study the spectral dependence and threshold behavior by using spectral slices at a fixed delay of 3 ps. Figure 2a shows the result for increasing occupation $\langle N \rangle$. We observe a strong bleach at the band gap transition, eventually giving way to net optical gain $\mu_i < 0$. The full collapse and even inversion of the lowest optical transition band upon strong photoexcitation are remarkable since they are not observed in the parent CdSe nanoplatelets.[5,7] Figure 2b shows the material gain $g_i(\lambda) = -\mu_i(\lambda)$ at 3 ps. The spectrum is initially confined to the region of 650 nm, where almost no linear absorption (dashed black line, Figure 2b) is present, only to blue shift toward 600 nm with a concomitant increase in magnitude, peaking at ca. 6000 cm^{-1}. Having normalized to obtain the material gain, we can compare these numbers to other reports such as those for

https://doi.org/10.1021/acs.nanolett.1c03501
Nano Lett. 2021, 21, 10062−10069

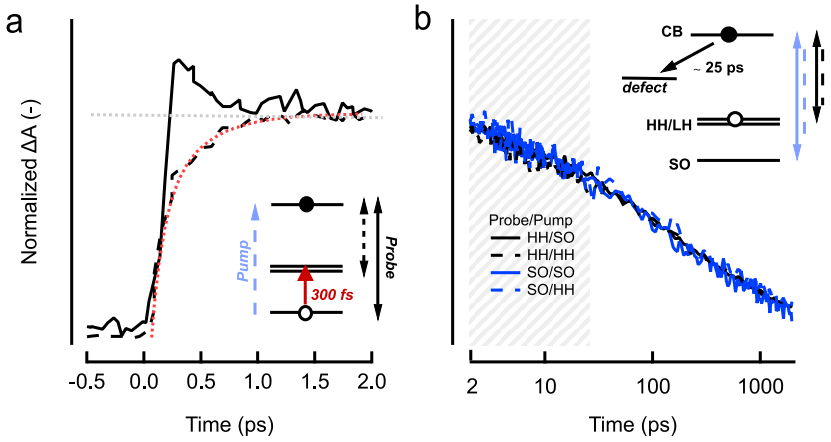

Figure 3. Dynamics of single electron−hole pairs in CdSe QRs. (a) Normalized ΔA traces probed at the HH/LH−CB transition (dashed line) and the SO/CB transition (solid line) after excitation at the SO/CB (510 nm) creating $\langle N \rangle = 0.5$. A double-exponential fit (dotted red line) reveals fast single-hole cooling (300 fs) from the SO to the HH/LH level(s). (b) Normalized ΔA kinetics at longer time delays, with a log scale for the time axis, probed at the HH/LH−CB and SO−CB transitions indicating that after initial fast hole cooling a common electron trap depletes the conduction band on a 25 ps time scale (gray shaded area). However, the weight of this component is limited to 30% of the total decay.

CdSe QDs (<3000 cm^{-1})[25] and CdSe nanoplatelets (>15.000 cm^{-1}).[5,7]

To evaluate the gain threshold, we plot in Figure 2c (bottom) the material gain at 660 nm for increasing electron−hole pair density $\langle N \rangle$, both for pumping resonantly with the HH/LH−CB (625 nm, red) and SO−CB (510 nm, green) transitions and for a scenario of hot excitation (400 nm, blue). For increasing density, we observe a crossover to net gain which occurs at $\langle N \rangle$ = 2.4, 3.5, 5.3 for 625, 510, and 400 nm pump wavelengths, respectively. The horizontal gray line in Figure 2c indicates the linear intrinsic absorption coefficient at 660 nm which is exceeded by a factor of 2, indicating strong spectral shifts.[25]

We finally proceed to study the gain lifetime, τ_G, defined as the time window for which $g_i(t)$ remains positive. Figure 2c (top) shows that τ_G is fluence-dependent yet independent of the initial pump wavelength. The gain lifetime reaches 160 ps, on par with reports on core-only CdSe quantum wells[5] yet shorter than record lifetimes for core/shell architectures such as CdSe/CdS quantum dots and wells.[6,25,26] Remarkably, no saturation of the gain lifetime is observed, suggesting that τ_G could further increase at higher fluence. The question remains as to whether this lifetime is capped by radiative or nonradiative processes, a point we will discuss below. Figure 2d shows slices of the fPL experiments at 3 ps for increasing $\langle N \rangle$ over a range similar to that for the TA experiments. We observe a strong asymmetric broadening of the PL relative to the steady state (vertical gray line), showing a progressive increase in the signal at short wavelengths (blue) and a moderate increase with clear saturation at longer ones (red).

Both the TA and fPL experiments show remarkable blue and red shifts of the bleach and luminescence spectra. Combined with this, we observe a full inversion of the absorption spectrum into a continuous, broad gain spectrum which is not observed in highly excitonic 2D materials.[7] To understand these effects and their impact on optical gain, we should first consider how net stimulated emission could develop in weakly confined semiconductors. A first and distinctively exciton-mediated mechanism was recently unveiled for CdSe nanoplatelets.[5] In this model, the fusion of mobile and weakly confined 2D excitons to energetically favorable (biexcitonic) molecules gives rise to net stimulated emission along the molecule-to-exciton recombination pathway. A hallmark of this mechanism is the formation of molecules with well-defined total angular momentum.[5] Experimentally, a circularly polarized pump−probe sequence $\sigma^+\sigma^+$ should generate unbound molecules with total angular momentum $F = 2$, whereas $\sigma^+\sigma^-$ is set to create a bound singlet molecular state ($F = 0$) by photon absorption from a single exciton state. Since possible molecular states are stabilized with a binding energy Δ_M relative to the single exciton states, one expects an induced absorption at a probe photon energy of $E_X - \Delta_M$ for the $\sigma^+\sigma^-$ sequence and the absence thereof in the $\sigma^+\sigma^+$ sequence. Figure 2f shows the result at 3 ps for such an experiment where the QRs were excited with polarization sequences as explained above. No difference is observed between the two pump−probe experiments, indicating that stable molecules cannot be formed in our QRs, thereby ruling out the excitonic gain mechanism.

A second mechanism for developing net gain is that found in many epitaxial quantum wells where charge carriers condense into an uncorrelated plasma-like state, leading to population inversion and net stimulated emission across the band gap (Figure 2e, bottom). The presence of a plasma state in 2D semiconductors normally leads to a red shift of the single-particle gap, called band gap renormalization (BGR).[27−29] The latter shifts the gain window toward lower energies, which is exactly what is observed in Figure 2b.

Further proof of a plasma state can be found in its peculiar dynamics at both early times and at later times. Before we continue to the high-density regime, we first assess the quality and intrinsic nature of the QRs through the single-charge pair dynamics.

Figure 3a shows the normalized TA traces probing the HH/LH−CB (dashed line) and SO−CB (solid line) transitions after excitation into the SO−CB (510 nm) manifold, hence creating a hot hole and a cold electron. Any discrepancy between both probe wavelengths would indicate hole dynamics, whereas common dynamics are to be linked to electrons.[30] At early times, we observe a common fast ingrowth scale indicative of fast occupation of the CB state by an electron. The slower, 300 ± 15 fs, ingrowth of HH/LH (dashed line) and decay of SO (solid line) indicate efficient

https://doi.org/10.1021/acs.nanolett.1c03501
Nano Lett. 2021, 21, 10062−10069

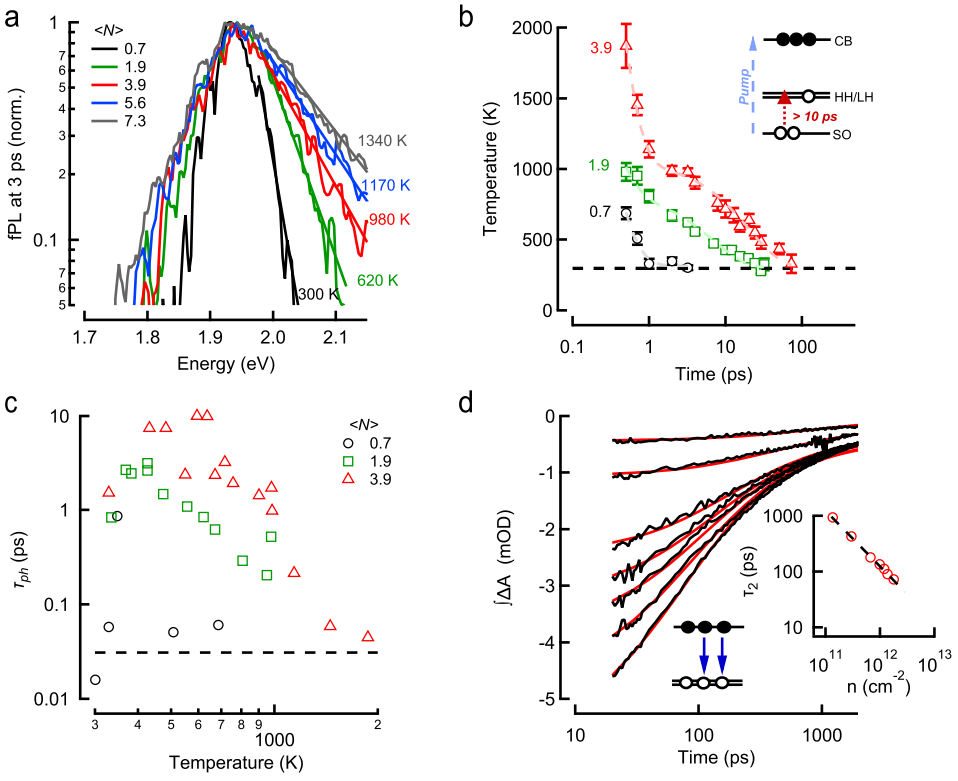

Figure 4. Dynamics of electron−hole pairs at high density. (a) fPL spectra at 3 ps plotted on an energy scale for excitation at 515 nm (2.4 eV) at increasing pair density $\langle N \rangle$. Solid lines indicate the single-exponential Boltzmann fit used to extract the carrier temperature from the high-energy side of the fPL spectra. (b) Extracted effective carrier temperature from the slope of the spectra in (a) for $\langle N \rangle$ = 0.7, 1.9, 3.9. Biexponential fits (dashed lines) are discussed in the main text. (c) LO−phonon emission time extracted from the cooling curves in (b) as a function of the effective carrier temperature. The dashed black line represents the expected theoretical value for electron−LO phonon scattering. (d) Decay of ΔA integrated across the HH/LH − CB bleach fitted with a second-order recombination model (red lines) for $\langle N \rangle$ between 0.5 and 6.9. The inset represents the two-body recombination time constant $\tau_2 = \frac{1}{k_2 n_0}$.

hole cooling between SO and HH/LH (Supporting Information).

Normalized after 2 ps, Figure 3b shows that all traces line up, indicating a loss of the common charge (i.e., electrons). As highlighted by the shaded region, we can identify two lifetimes of the signal decay: a fast but fluence-independent scale spanning a time window of ca. 25 ps, followed by a slower channel that accounts for >70% of the initial population. Notably, a similar set of observations was made by Xiao et al., who reported a substantially faster short lifetime (ca. 6 ps) and a much larger weight of the short-lived component.[11] The moderate trapping, both in relative weight and absolute time scale, in our QRs indicates their excellent surface passivation. The second regime, extending beyond 25 ps, shows a fluence-dependent lifetime, a point we will come back to further.

Next, we can proceed to understand what happens at increasing density. Looking back at Figures 1e and 2d, we observe strong luminescence blue-shifted from the steady-state PL spectrum in the first 10 ps time window, which indicates that charge carriers occupy a continuous band of high-lying energy levels.

It is well established that the slope of the luminescence at high photon energy can be described using a Boltzmann tail $e^{-E/k_B T_{eff}}$,[31−33] with T_{eff} being the effective carrier temperature. Using this approach, Figure 4a shows a progressive increase of T_{eff} with $\langle N \rangle$. In the same way, from the change in the fPL slope as a function of time, we can extract the cooling curves $T(t)$ for increasing $\langle N \rangle$. As shown in Figure 4b, at low density, the carrier temperature drops monoexponentially on a subpicosecond time scale (τ_0 = 270 ± 30 fs), matching the hole-cooling kinetics reported in Figure 3a. However, at increased pair densities, the temperature increases at early times and remains overheated until nearly 100 ps. A qualitative biexponential fit to the cooling curve at $\langle N \rangle$ = 1.9 ($\langle N \rangle$ = 3.9) reveals an additional component, τ_1 = 7 ± 1 ps (τ_1 = 21 ± 2 ps) (Supporting Information). Charge cooling in polar semiconductors such as CdSe takes place by rapid optical phonon emission. However, it is exactly this rapid phonon emission which could overheat the phonon modes at high carrier density, leading to a lingering effective high carrier temperature T_{eff}. To be more quantitative, we extract the average time required to emit a phonon τ_{ph} from the slope of the cooling curves $T(t)$[34] (Supporting Information 3.10). As shown in Figure 4c, at low density τ_{ph} is essentially constant at around 50 fs, matching a theoretical estimate for CdSe (Supporting Information 3.10). At higher electron−hole pair densities, τ_{ph} markedly increases to nearly 10 ps. Similar observations were made on various polar semiconductors such as perovskites[35,36] and for various topologies of Cd-chalcogenides.[7,14,15,37] We note that the measured high carrier temperatures are incompatible with the thermal stability of excitons or biexcitons, again pointing to a plasma state.

After a few tens of picoseconds, the charge cooling is complete and the limited linear electron trapping (25 ps) is finished. Beyond this time frame, we observe that the recombination is dependent on the pump fluence (Figure

https://doi.org/10.1021/acs.nanolett.1c03501
Nano Lett. 2021, 21, 10062−10069

4d). In general, carrier recombination can be modeled using a mixed first- and second-order process:

$$-\frac{dn}{dt} = k_1 n + k_2 n^2 \approx k_2 n^2$$

However, in the range beyond 25 ps, the (electron) trapping processes summarized by k_1 can be neglected. As shown in Figure 4d, a fit with k_2 as a global parameter matches the ΔA traces for $\langle N \rangle$ between 0.5 and 6.9. The fit yields a second-order recombination rate of $k_2 = (7.7 \pm 0.1) \times 10^{-3}$ cm^2/s, which is in line with various reports.[38−41] However, it exceeds those values found for thinner 4.5 ML CdSe NPLs by an order of magnitude ($k_2 = 0.13 \times 10^{-3}$, 0.97×10^{-3} cm^2/s),[7,42] most likely because the process considered here for unbound charge carriers entices a radiative electron−hole recombination process, which contrasts with Auger-type exciton−exciton annihilation. Our analysis implies that the limited gain lifetime is hence not due to nonradiative losses but is due to fast radiative recombination, an important difference with nanoplatelets or quantum dots and a feat also observed in weakly confined perovskites.[35,43] From k_2, we can calculate a density-dependent two-body recombination time $\tau_2 = \frac{1}{k_2 n_0}$ (Figure 4d) which varies between 0.1 and 1 ns.

We obtained a set of intrinsic observations on QRs which point toward a situation where not excitons but a hot plasma state is present, giving rise to peculiar photophysics that is unexpected for the case of a confined 2D material. Both the full exciton saturation and inversion, the absence of polarization-resolved transitions, and the high carrier temperatures make exciton-based gain unlikely. Clearly, the reduced confinement in the out-of-plane direction compared to thin nanoplatelets, combined with strong carrier−carrier interactions evidenced by strong band gap renormalization and comparatively fast radiative bimolecular recombination, strongly reduces the excitonic nature of the fundamental excitations in QRs. We did not observe any correlation between the QR's unique $g = 1$ topology and the ultrafast phenomena discussed here which could be due to limited rotational symmetry, as observed similarly by Hartmann et al.,[10] or carrier localization at room temperature.[44] Overall, CdSe QRs at room temperature behave more as classical quantum wells, providing a unique platform for studying unbound charge carriers in colloidal materials.

■ ASSOCIATED CONTENT

Supporting Information

The Supporting Information is available free of charge at https://pubs.acs.org/doi/10.1021/acs.nanolett.1c03501.

Quantum ring synthesis and structural characterization, a discussion of the linear and nonlinear optical properties, and a description and modeling of the ultrafast experiments (PDF)

■ AUTHOR INFORMATION

Corresponding Author

Pieter Geiregat − *Physics and Chemistry of Nanostructures, Department of Chemistry, Center for Nano and Biophotonics, and Physics and Chemistry of Nanostructures, Department of Chemistry, Ghent University, B-9000 Gent, Belgium;* orcid.org/0000-0001-7217-8738; Email: Pieter.Geiregat@Ugent.be

Authors

Carmelita Rodà − *Physics and Chemistry of Nanostructures, Department of Chemistry and Center for Nano and Biophotonics, Ghent University, B-9000 Gent, Belgium*

Bastiaan B. V. Salzmann − *Debye Institute for Nanomaterials Science, Utrecht University, 3508 TA Utrecht, The Netherlands;* orcid.org/0000-0002-8055-4681

Isabella Wagner − *School of Chemical and Physical Sciences and MacDiarmid Institute for Advanced Materials and Nanotechnology, Victoria University of Wellington, Wellington 6012, New Zealand*

Yera Ussembayev − *Center for Nano and Biophotonics and Liquid Crystals and Photonics Research Group, Department of Information Technology, Ghent University, B-9000 Gent, Belgium;* orcid.org/0000-0002-4779-9046

Kai Chen − *MacDiarmid Institute for Advanced Materials and Nanotechnology and Robinson Research Institute, Victoria University of Wellington, Wellington 6012, New Zealand; The Dodd-Walls Centre for Photonic and Quantum Technologies, University of Otago, Dunedin 9010, New Zealand*

Justin M. Hodgkiss − *School of Chemical and Physical Sciences and MacDiarmid Institute for Advanced Materials and Nanotechnology, Victoria University of Wellington, Wellington 6012, New Zealand;* orcid.org/0000-0002-9629-8213

Kristiaan Neyts − *Center for Nano and Biophotonics and Liquid Crystals and Photonics Research Group, Department of Information Technology, Ghent University, B-9000 Gent, Belgium;* orcid.org/0000-0001-5551-9772

Iwan Moreels − *Center for Nano and Biophotonics and Physics and Chemistry of Nanostructures, Department of Chemistry, Ghent University, B-9000 Gent, Belgium;* orcid.org/0000-0003-3998-7618

Daniel Vanmaekelbergh − *Debye Institute for Nanomaterials Science, Utrecht University, 3508 TA Utrecht, The Netherlands*

Complete contact information is available at: https://pubs.acs.org/10.1021/acs.nanolett.1c03501

Author Contributions

C.R and B.B.V.S. contributed equally to the manuscript. B.B.V.S. synthesized the QRs and characterized them using microscopy, and both C.R. and B.B.V.S. performed TA measurements and analyzed the data. Y.U. and K.N. provided the field calculations. K.C., J.M.H., and I.W. provided the femtosecond PL measurements. P.G., I.M., and D.V. supervised the research. C.R. wrote the paper with P.G. and B.B.V.S.

Notes

The authors declare no competing financial interest.

■ ACKNOWLEDGMENTS

P.G. acknowledges support from FWO-Vlaanderen. This project has received funding from the European Research Council (ERC) under the European Union's Horizon 2020 research and innovation program (grant agreement no. 714 876 PHOCONA). B.B.V.S. and D.V. acknowledge the Dutch NWO for financial support via TOP-ECHO grant no. 715.016.002. D.V. acknowledges financial support from the European ERC Council, ERC Advanced grant 692 691 "First Step".

REFERENCES

(1) Ithurria, S.; Tessier, M. D.; Mahler, B.; Lobo, R. P. S. M.; Dubertret, B.; Efros, A. L. Colloidal nanoplatelets with two-dimensional electronic structure. *Nat. Mater.* **2011**, *10*, 936−941.

(2) Pietryga, M.; Park, Y.-s.; Lim, J.; Fidler, A. F.; Bae, W. K.; Brovelli, S.; Klimov, V. I. Spectroscopic and Device Aspects of Nanocrystal Quantum Dots. *Chem. Rev.* **2016**, *116*, 10513−10622.

(3) Scott, R.; Heckmann, J.; Prudnikau, A. V.; Antanovich, A.; Mikhailov, A.; Owschimikow, N.; Artemyev, M.; Climente, J. I.; Woggon, U.; Grosse, N. B.; Achtstein, A. W. Directed Emission of CdSe Nanoplatelets Originating from Strongly Anisotropic 2D Electronic Structure. *Nat. Nanotechnol.* **2017**, *12*, 1155−1160.

(4) Guzelturk, B.; Pelton, M.; Olutas, M.; Demir, H. V. Giant Modal Gain Coefficients in Colloidal II-VI Nanoplatelets. *Nano Lett.* **2019**, *19*, 277−282.

(5) Geiregat, P.; Tomar, R.; Chen, K.; Singh, S.; Hodgkiss, J. M.; Hens, Z. Thermodynamic Equilibrium between Excitons and Excitonic Molecules Dictates Optical Gain in Colloidal CdSe Quantum Wells. *J. Phys. Chem. Lett.* **2019**, *10*, 3637−3644.

(6) Altintas, Y.; Gungor, K.; Gao, Y.; Sak, M.; Quliyeva, U.; Bappi, G.; Mutlugun, E.; Sargent, E. H.; Demir, H. V. Giant Alloyed Hot Injection Shells Enable Ultralow Optical Gain Threshold in Colloidal Quantum Wells. *ACS Nano* **2019**, *13*, 10662−10670.

(7) Tomar, R.; Kulkarni, A.; Chen, K.; Singh, S.; Thourhout, D. V.; Hodgkiss, J. M.; Siebbeles, L. D. A.; Hens, Z.; Geiregat, P. Charge Carrier Cooling Bottleneck Opens Up Nonexcitonic Gain Mechanisms in Colloidal CdSe Quantum Wells. *J. Phys. Chem. C* **2019**, *123*, 9640−9650.

(8) Fedin, I.; Talapin, D. V. Colloidal CdSe Quantum Rings. *J. Am. Chem. Soc.* **2016**, *138*, 9771−9774.

(9) Salzmann, B. B.; Vliem, J. F.; Maaskant, D. N.; Post, L. C.; Li, C.; Bals, S.; Vanmaekelbergh, D. From CdSe Nanoplatelets to Quantum Rings by Thermochemical Edge Reconfiguration. *Chem. Mater.* **2021**, *33*, 6853−6859.

(10) Hartmann, N. F.; Otten, M.; Fedin, I.; Talapin, D.; Cygorek, M.; Hawrylak, P.; Korkusinski, M.; Gray, S.; Hartschuh, A.; Ma, X. Uniaxial transition dipole moments in semiconductor quantum rings caused by broken rotational symmetry. *Nat. Commun.* **2019**, *10*, 3253.

(11) Xiao, J.; et al. Optical and electronic properties of colloidal CdSe quantum rings. *ACS Nano* **2020**, *14*, 14740−14760.

(12) Flórez, F. G.; Kulkarni, A.; Siebbeles, L. D. A.; Stoof, H. T. C. Explaining Observed Stability of Excitons in Highly Excited CdSe Nanoplatelets. *Phys. Rev. B: Condens. Matter Mater. Phys.* **2019**, *100*, 245−302.

(13) Li, Q.; Lian, T. Area- and Thickness-Dependent Biexciton Auger Recombination in Colloidal CdSe Nanoplatelets: Breaking the "Universal Volume Scaling Law. *Nano Lett.* **2017**, *17*, 3152−3158.

(14) Sippel, P.; Albrecht, W.; Bok, J. C. V. D.; Dijk-moes, R. J. A. V.; Hannappel, T.; Eichberger, R.; Vanmaekelbergh, D. Femtosecond Cooling of Hot Electrons in CdSe Quantum-Well Platelets. *Nano Lett.* **2015**, *15*, 2409−2416.

(15) Diroll, B. T.; Talapin, D. V.; Schaller, R. D. Violet-to-Blue Gain and Lasing from Colloidal CdS Nanoplatelets: Low-Threshold Stimulated Emission Despite Low Photoluminescence Quantum Yield. *ACS Photonics* **2017**, *4*, 576−583.

(16) She, C.; Fedin, I.; Dolzhnikov, D. S.; Dahlberg, P. D.; Engel, G. S.; Schaller, R. D.; Talapin, D. V. Red, Yellow, Green, and Blue Amplified Spontaneous Emission and Lasing Using Colloidal CdSe Nanoplatelets. *ACS Nano* **2015**, *9*, 9475−9485.

(17) Grim, J. Q.; Christodoulou, S.; Di Stasio, F.; Krahne, R.; Cingolani, R.; Manna, L.; Moreels, I. Continuous-wave biexciton lasing at room temperature using solution-processed quantum wells. *Nat. Nanotechnol.* **2014**, *9*, 891−895.

(18) Christodoulou, S.; Climente, J. I.; Planelles, J.; Brescia, R.; Prato, M.; Martin-Garcia, B.; Khan, A. H.; Moreels, I. Chloride-Induced Thickness Control in CdSe Nanoplatelets. *Nano Lett.* **2018**, *18*, 6248−6254.

(19) Ussembayev, Y. Y.; Hens, Z.; Neyts, K. Contrasting Anisotropy of Light Absorption and Emission by Semiconductor Nanoparticles. *ACS Photonics* **2019**, *6*, 1146−1152.

(20) Ussembayev, Y. Y.; Zawacka, N. K.; Strubbe, F.; Hens, Z.; Neyts, K. Waveguiding of Photoluminescence in a Layer of Semiconductor Nanoparticles. *Nanomaterials* **2021**, *11*, 683.

(21) Hens, Z.; Moreels, I. Light Absorption by Colloidal Semiconductor Quantum Dots. *J. Mater. Chem.* **2012**, *22*, 10406−10415.

(22) Ji, B.; Rabani, E.; Efros, A. L.; Vaxenburg, R.; Ashkenazi, O.; Azulay, D.; Banin, U.; Millo, O. Dielectric Confinement and Excitonic Effects in Two-Dimensional Nanoplatelets. *ACS Nano* **2020**, *14*, 8257−8265.

(23) Zelewski, S. J.; Nawrot, K. C.; Zak, A.; Gladysiewicz, M.; Nyk, M.; Kudrawiec, R. Exciton Binding Energy of Two-Dimensional Highly Luminescent Colloidal Nanostructures Determined from Combined Optical and Photoacoustic Spectroscopies. *J. Phys. Chem. Lett.* **2019**, *10*, 3459−3464.

(24) Chen, K.; Gallaher, J. K.; Barker, A. J.; Hodgkiss, J. M. Transient grating photoluminescence spectroscopy: An ultrafast method of gating broadband spectra. *J. Phys. Chem. Lett.* **2014**, *5*, 1732−1737.

(25) Bisschop, S.; Geiregat, P.; Aubert, T.; Hens, Z. The Impact of Core/Shell Sizes on the Optical Gain Characteristics of CdSe/CdS Quantum Dots. *ACS Nano* **2018**, *12*, 9011−9021.

(26) Park, Y.-S.; Roh, J.; Diroll, B. T.; Schaller, R. D.; Klimov, V. I. Colloidal quantum dot lasers. *Nat. Rev. Mater.* **2021**, *6*, 382−401.

(27) Masumoto, Y.; Fluegel, B.; Meissner, K.; Paul, A. Band-gap renormalization excited CdSe. *J. Cryst. Growth* **1992**, *117*, 732−737.

(28) Sarma, S. D.; Yang, E. Band-gap renormalization in semiconductor quantum wells. *Phys. Rev. B: Condens. Matter Mater. Phys.* **1990**, *41*, 8288−8294.

(29) Weber, C.; Klingshirn, C.; Chemla, D.; Miller, D.; Cunningham, J.; Ell, C. Gain Measurements and Band-gap renormalization in GaAs/AlGaAs Multiple Quantum Well Structures. *Phys. Rev. B: Condens. Matter Mater. Phys.* **1988**, *38*, 12748.

(30) Khan, A. H.; Pinchetti, V.; Tanghe, I.; Dang, Z.; Hens, Z.; Thourhout, D. V.; Geiregat, P.; Brovelli, S.; Moreels, I. Tunable and Efficient Red to Near-Infrared Photoluminescence by Synergistic Exploitation of Core and Surface Silver Doping of CdSe Nanoplatelets. *Chem. Mater.* **2019**, *31*, 1450−1459.

(31) Pelton, M.; Ithurria, S.; Schaller, R. D.; Dolzhnikov, D. S.; Talapin, D. V. Carrier cooling in colloidal quantum wells. *Nano Lett.* **2012**, *12*, 6158−63.

(32) Ryan, J. F.; Taylor, R. A.; Turberfield, A. J.; Maciel, A.; Worlock, J. M.; Gossard, A. C.; Wiegmann, W. Time-Resolved Photoluminescence of Two-Dimensional Hot Carriers in GaAs-AlGaAs Heterostructures. *Phys. Rev. Lett.* **1984**, *53*, 1841−1844.

(33) von der Linde, D.; Lambrich, R. Direct Measurement of Hot-Electron Relaxation by Picosecond Spectroscopy. *Phys. Rev. Lett.* **1979**, *42*, 1090−1093.

(34) Yang, Y.; Ostrowski, D. P.; France, R. M.; Zhu, K.; van de Lagemaat, J.; Luther, J. M.; Beard, M. C. Observation of a hot-phonon bottleneck in lead-iodide perovskites. *Nat. Photonics* **2016**, *10*, 53−59.

(35) Geiregat, P.; Maes, J.; Chen, K.; Drijvers, E.; De Roo, J.; Hodgkiss, J. M.; Hens, Z. Using Bulk-like Nanocrystals To Probe Intrinsic Optical Gain Characteristics of Inorganic Lead Halide Perovskites. *ACS Nano* **2018**, *12*, 10178−10188.

(36) Price, M.; Butkus, J.; Jellicoe, T.; Sadhanala, A.; Briane, A.; Halpert, J.; Broch, K.; Hodgkiss, J.; Friend, R.; Deschler, F. Hot Carrier Cooling and Photo-induced Refractive Index Changes in Organic-Inorganic Lead Halide Perovskites. *Nat. Commun.* **2015**, *6*, 8420.

(37) Saito, H.; Göbel, E. Picosecond spectroscopy of highly excited Cds. *Phys. Rev. B: Condens. Matter Mater. Phys.* **1985**, *31*, 2360−2369.

(38) Kumar, N.; Cui, Q.; Ceballos, F.; He, D.; Wang, Y.; Zhao, H. Exciton-exciton annihilation in $MoSe_2$ monolayers. *Phys. Rev. B: Condens. Matter Mater. Phys.* **2014**, *89*, 125427.

https://doi.org/10.1021/acs.nanolett.1c03501
Nano Lett. 2021, 21, 10062−10069

(39) Sun, D.; Rao, Y.; Reider, G. A.; Chen, G.; You, Y.; Brézin, L.; Harutyunyan, A. R.; Heinz, T. F. Observation of Rapid Exciton−Exciton Annihilation in Monolayer Molybdenum Disulfide. *Nano Lett.* **2014**, *14*, 5625−5629.
(40) Yuan, L.; Huang, L. Exciton dynamics and annihilation in WS2 2D semiconductors. *Nanoscale* **2015**, *7*, 7402−7408.
(41) Delport, G.; Chehade, G.; Lédée, F.; Diab, H.; Milesi-Brault, C.; Trippé-Allard, G.; Even, J.; Lauret, J.-S.; Deleporte, E.; Garrot, D. Exciton−Exciton Annihilation in Two-Dimensional Halide Perovskites at Room Temperature. *J. Phys. Chem. Lett.* **2019**, *10*, 5153−5159.
(42) Kunneman, L. T.; Tessier, M. D.; Heuclin, H.; Dubertret, B.; Aulin, Y. V.; Grozema, F. C.; Schins, J. M.; Siebbeles, L. D. A. Bimolecular Auger Recombination of Electron−Hole Pairs in Two-Dimensional CdSe and CdSe/CdZnS Core/Shell Nanoplatelets. *J. Phys. Chem. Lett.* **2013**, *4*, 3574−3578.
(43) Baghani, E.; O'Leary, S. K.; Fedin, I.; Talapin, D. V.; Pelton, M. Auger-Limited Carrier Recombination and Relaxation in CdSe Colloidal Quantum Wells. *J. Phys. Chem. Lett.* **2015**, *6*, 1032−1036.
(44) Geiregat, P.; Rodà, C.; Tanghe, I.; Singh, S.; Giacomo, D.; Lebrun, D.; Grimaldi, G.; Maes, J.; Van, D.; Moreels, I.; Houtepen, A. J.; Hens, Z. Localization-Limited Exciton Oscillator Strength in Colloidal CdSe Nanoplatelets Revealed by The Optically Induced Stark Effect. *Light: Sci. Appl.* **2021**, *10*, 112.

https://doi.org/10.1021/acs.nanolett.1c03501
Nano Lett. 2021, 21, 10062−10069